Journal of Hazardous Materials 396 (2020) 122605

Contents lists available at ScienceDirect

Journal of Hazardous Materials

journal homepage: www.elsevier.com/locate/jhazmat

Cooperative application of transcriptomics and ceRNA hypothesis: LncRNA-107052630/miR-205a/G0S2 crosstalk is involved in ammonia-induced intestinal apoptotic injury in chicken

Wang Shengchen[a], Wang Wei[a], Li Xiaojing[a], Zhao Xia[a], Wang Yue[a], Zhang Hongfu[b,*], Xu Shiwen[a,c,**]

[a] College of Veterinary Medicine, Northeast Agricultural University, Harbin 150030, PR China
[b] State Key Laboratory of Animal Nutrition, Institute of Animal Sciences, Chinese Academy of Agricultural Sciences, Beijing 100193, PR China
[c] Key Laboratory of the Provincial Education Department of Heilongjiang for Common Animal Disease Prevention and Treatment, College of Veterinary Medicine, Northeast Agricultural University, Harbin, 150030, PR China

GRAPHICAL ABSTRACT

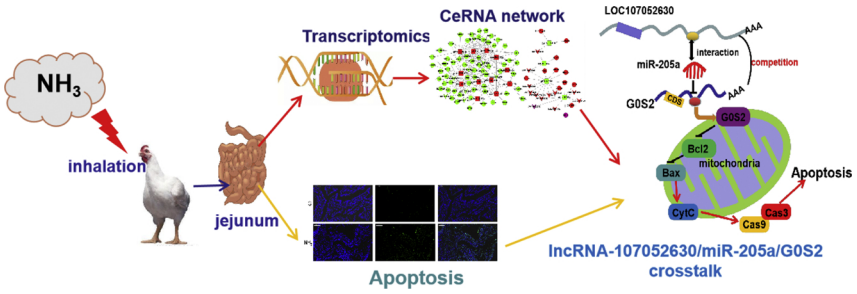

ARTICLE INFO

Editor: R. Debora

Keywords:
Ammonia
jejunum
Apoptosis
ceRNA
Transcriptome

ABSTRACT

Ammonia (NH_3), as a harmful gas from agricultural production, plays an important role in air pollution, such as haze. Although numerous researchers have paid attention to health damage through NH_3 inhalation, the exhaustive mechanism of NH_3 induced intestinal toxicity remains unclear. A genes crosstalk named competing endogenous RNAs (ceRNA) can explain many regulatory manners from the molecular perspective. However, few studies have attempted to interpret the injury mechanism of air pollutants to the organism via ceRNA theory. Here, we thoroughly investigated the lncRNA-associated-ceRNA mechanism in jejunum samples from a 42-days-old NH_3-exposed chicken model through deep RNA sequencing. We observed the occurrence of apoptosis in jejunum, obtained 46 significantly dysregulated lncRNAs and 30 dysregulated miRNAs, and then constructed lncRNA-associated-ceRNA networks in jejunum. Importantly, a network regulating G0S2 in NH_3-induced apoptosis was discovered. Research results showed that G0S2 was upregulated in jejunum of NH_3-exposed group and was associated with activation of the mitochondrial apoptosis pathway. G0S2 antagonized the anti-apoptotic effect of Bcl2, which could be reversed by miR-205a. Meanwhile, lncRNA-107052630 acted as ceRNA to affect G0S2 function. These data provide new insight for revealing the biological effect of NH_3 toxicity, as well as the environmental research.

* Corresponding author at: Institute of Animal Sciences, Chinese Academy of Agricultural Sciences, Beijing 100193, PR China.
** Corresponding author at: College of Veterinary Medicine, Northeast Agricultural University, Harbin, 150030, PR China.
E-mail addresses: zhanghongfu@caas.cn (H. Zhang), shiwenxu@neau.edu.cn (S. Xu).

https://doi.org/10.1016/j.jhazmat.2020.122605
Received 14 January 2020; Received in revised form 24 March 2020; Accepted 26 March 2020
Available online 18 April 2020

1. Introduction

The value of agricultural exports has rapidly increased over the past decade and is driven by economic globalization and increasing demand of developing countries. However, when ships filled with meats and grains leave the port, a variety of pollutions are left behind, especially ammonia (NH_3) (Stokstad, 2014). This colorless and irritating gas is mainly derived from feces of farm livestock and ammonia-based liquid fertilizers, can interact with nitrogen oxides to form the main component of haze, thus threatening human and animal health (Plautz, 2018; Liu et al., 2019). Accumulating evidence has confirmed that the annual premature mortality caused by particulate matter concentrations ($PM_{2.5}$) from NH_3 emissions increased the hidden cost of agricultural exports in the U.S. (Van Damme et al., 2018). NH_3 can directly burn the respiratory system and cause lesions in other tissues through entering the blood circulation. High concentration of atmospheric NH_3 could overcome liver clearance capacity, resulting in chronic hepatic injury, hyperammonemia and cerebral edema (Adeva et al., 2012; Zhang et al., 2015). Chen et al. proved that NH_3 induced inflammatory injury in chicken thymuses by disrupting the antioxidant system and promoting the expression of inflammatory factors (IL-1β, IL-6, IL-8, and iNOS) (Chen et al., 2019a). Intestine is a target organ of a variety of air pollutants. Concentrated ambient particles could alter the diversity of gut microorganisms, thus inducing inflammation in the intestinal tract in mice (Mutlu et al., 2018). However, because the intestine is an important source of NH_3 production in organisms, the effect of exogenous NH_3 on the intestine has long been ignored. Our micromorphological result showed that NH_3 exposure could cause intestinal microvilli deficiency through disrupting microtubule activity in chicken (Wang et al., 2019a). This finding suggests that the mechanism of intestinal damage caused by NH_3 must be further explored.

Abnormal cell death is regard as an inherent hallmark of animals that are undergoing pathological changes or subjected to harmful stimulation. NH_3 exposure can cause apoptosis in a variety of tissues (Jin et al., 2017). It has been reported that NH_3 exposure-induced oxidative stress could result in apoptosis in the liver of black tiger shrimp (*Penaeus monodon*) (Liang et al., 2016). Furthermore, in vitro experiments clarified that GSM06 cells treated with ammonium chloride (NH_4Cl) to simulate a NH_3 induced-gastric mucous injury model also showed the release of cytochrome c (CytC) from mitochondria, followed by caspase-9 (Cas9) activation and caspase-3 (Cas3) cleavage, as well as the apoptotic phenotype of nuclear pyknosis (Suzuki et al., 2002). MicroRNAs (miRNAs) are small non-coding RNAs that posttranslationally regulate protein-coding messenger RNAs (mRNAs) by binding to target sequences located at mRNA 3′-UTR, thus blocking mRNA translation and protein production (Yang et al., 2018). Recent findings identify an intricate interplay among mRNAs and non-coding RNAs, such as circular RNAs (cirRNAs) and long non-coding RNAs (lncRNAs). These non-coding RNAs have ability to act as molecular sponges of microRNAs or competing endogenous RNAs (ceRNAs), share microRNA response elements (MREs) with mRNA 3′-UTR, modulating the expression of mRNAs targeted by microRNAs. This RNA crosstalk represents a novel layer of gene regulation that plays crucial roles in animal metabolism, reproduction, cell death, disease and response to irritation (Tay et al., 2014; Karreth and Pandolfi, 2013; Xu et al., 2016). Gao et al. found that under heavy metal cadmium stress, lncRNA Metallothionein 1D, Pseudogene (lncRNA MT1DP) was quickly reinforced to function as a ceRNA competitive binding miR-214, leading to calcium influx and apoptosis in liver regulated by Metallothionein 1H (MT1H) activated RhoC-CCN1/2-AKT signaling transduction (Gao et al., 2018). In addition, lncRNA 3037 promoted apoptosis and necroptosis of broiler trachea by sponging miR-15a to regulate Bcl2 and A20 expression during hydrogen sulfide (H_2S) exposure (Li et al., 2019). Generally speaking, in the mitochondrial apoptosis pathway, anti-apoptotic gene Bcl2 plays a key role in Bcl2 homology (BH) domains, the so-called death domain, which interacts with the pro-apoptotic gene Bax to inhibit apoptosis (Hoetelmans et al., 2000). A recent study identified G0/G1 switch gene 2 (G0S2) as a new apoptosis regulator that can specifically interact with Bcl2 and promote apoptosis by preventing the formation of Bcl2/Bax heterodimers (Kusakabe et al., 2010; Welch et al., 2009). In addition, G0S2 represses PI3K/mTOR signaling and functions as a tumor suppressor in breast cancer (Yim et al., 2017, 2016). However, studies on how to regulate the activity of G0S2 have not been reported in detail.

Transcriptomics or global gene expression analysis in the research of adverse health effects associated with toxicants exposure has potential application value (Du et al., 2017). Chickens are extensively employed as model animals to study the biotoxicity of exogenous pollutants.Thus, in the present study, broiler chicken was used as research object to assess whether ceRNA mechanisms play a role in intestinal injury induced by NH_3. We established lncRNA-associated-ceRNA networks by screening and analyzing the differentially expressed RNA based on transcriptome results. Mechanistic investigations demonstrated that lncRNA-107052630 acts as a ceRNA, serving as a sink for miR-205a that subsequently activates G0S2 and the mitochondrial apoptosis pathway. The results of our study will provide a technical reference regarding research methods of intestinal toxicity of NH_3 and have large regulatory implications for ecological risk assessment of human health.

2. Materials and methods

2.1. Animals and experimental design

Eighty broiler chickens (1-day-old) were randomly divided into two groups (forty chickens/group) named the C group and the NH_3-exposed group, respectively. Chickens from both groups were transferred to environmentally controlled exposure chambers (chamber C and chamber N) and housed in individual cages under standard brooding practices. Concentrated NH_3 was delivered in a whole-body animal exposure chamber at $20 \pm 0.5\,mg/m^3$ during 1–21 days and $45 \pm 0.5\,mg/m^3$ during the 22–42 days (Shi et al., 2019). Meanwhile, we used LumaSense Photoacoustic Field Gas-Monitor Innova-1412 (Santa Clara, CA, USA) to monitor NH_3 concentrations of chambers belong to C and NH_3 groups continuously. Water and food were offered ad libitum by conventional feeding methods. Chickens were euthanized on the 42nd day of feeding. Then, the jejunum was extracted quickly, washed with normal saline and fixed with 4% paraformaldehyde or stored at – 80 °C for further experiment. The Animal Care and Use Committee of Northeast Agricultural University (SRM-11) approved all procedures used in the present study.

2.2. TUNEL staining

After removing the jejunums from C and NH_3 groups of chicken, the jejunal tissues were rinsed with normal saline and exposed to immersion fixation for 24 h at 4 °C in 4% paraformaldehyde. Then, 5 μm paraffin-embedded sections were generated from the jejunum tissues. An in situ apoptosis detection kit (Roche, Penzberg, Germany) was used for TdT-mediated dUTP Nick-End Labeling (TUNEL) staining. In brief, jejunum sections were incubated in the permeabilization solution and treated with the TUNEL reaction mixture. Subsequently, 10 μg/mL 4, 6-diamidino-2-phenylindole (DAPI) was used to stain and localize the nuclei of cells in the intestinal section in a humidified dark chamber. Using a scanning confocal microscope (Olympus FluoView FV1000), all intestinal nuclei were stained blue by DAPI, and the observed green-stained cells were proved to be apoptotic cells based on TUNEL result.

2.3. miRNA and lncRNA sequencing

Jejunal tissues of chicken from C group and NH3 group (n = 3/group) were used for miRNA and lncRNA sequencing. Samples from these two groups were lysed using Trizol Reagent (Invitrogen, Carlsbad,

CA, USA), and total RNA was obtained according to the manufacturer's instructions. We measured the purity of RNA using a NanoPhotometer® spectrophotometer (IMPLEN, CA, USA) and the quantity of RNA was detected using a Qubit® RNA Assay Kit in Qubit® 2.0 Flurometer (Life Technologies, CA, USA). A total amount of 1 μg RNA (RNA's RIN value > 7) per sample was used as input material for the RNA sample preparations. For lncRNA sequencing, after removing ribosomal RNA (rRNA) from total RNA using a Epicentre Ribo-zero™ rRNA Removal Kit (Epicentre, USA) and cleaning up rRNA free residue via ethanol precipitation, the sequencing libraries were generated using the NEBNext® Ultra Directional RNA Library Prep Kit for Illumina® (NEB, USA) with rRNA-depleted RNA following the manufacturer's recommendations. First, in the reaction buffer used in second strand cDNA synthesis, double-stranded cDNA was synthesized and dTTPs were replaced with dUTPs. Second, cDNA fragments preferentially 150 ~ 200 bp in length were selected from the library fragments purified by AMPure XP system (Beckman Coulter, Beverly, USA). Third, before performing PCR, size-selected and adaptor-ligated cDNA was reacted with 3 μL USER Enzyme (NEB, USA) at 37 °C for 15 min followed by 5 min at 95 °C. Then, PCR was performed with Phusion High-Fidelity DNA polymerase, Universal PCR primers, and Index (X) Primer. Finally, PCR products were purified using the AMPure XP system, and library quality was assessed on the Agilent Bioanalyzer 2100 system. For miRNA sequencing, RNA from two groups of jejunums was used as input material for microRNA library preparation. Sequencing libraries were obtained used the NEBNext® Multiplex Small RNA Library Prep Set for Illumina® (NEB, USA) following the manufacturer's recommendations. After enrichment for 16–32 nt small RNAs, multiplex adaptor ligation, reverse transcription primer hybridization, reverse transcription reaction and PCR amplification, cDNA constructs were purified and loaded on the Bioanalyzer 2100 system.

2.4. Quality control, reads mapping and differential expression analysis

We first processed Raw reads in the fastq format via in-house Perl scripts. After deleting reads with low quality, sequences containing adapters, reads containing ploy-N and empty reads from raw reads, we obtained the clean reads. Subsequently, the GC content of clean reads was calculated, and all the downstream analyses were based on high-quality clean data. For lncRNA mapping, the obtained clean reads were mapped to the reference genome of chicken that was directly downloaded from a genome website. Bowtie v2.2.3 was used to establish the index of the reference genome, and paired-end clean reads were aligned to the reference genome using TopHat v2.0.12. For miRNA mapping, after removing identical sequences, the clean reads from 18 to 32 nt were counted and mapped to the chicken genome (version miRbase V1.0) to annotate the location in the chromosomes using BWA (http://bio-bwa.sourceforge.net/). In addition, assembled unique sequences were identified using Rfam database 10.1. We used HTSeq (https://htseq.readthedocs.io/en/release_0.9.1/) to count the number of mapped reads. Subsequently, the FPKM of each gene was calculated according to the gene length and read count mapped to this gene. EB-Seq was applied to perform differential expression analyses of two groups (three biological replicates per group). Routine statistical assessment using EB-Seq combined with fold change (FC) and false discovery rate (FDR) was performed to determine the differentially expressed lncRNAs (DE-lncRNAs) or miRNAs (DE-miRNAs) (Fold Change > 1.5; FDR < 0.05). The obtained DE-lncRNAs or DE-miRNAs were used to construct heat map through heatmap.2 function in gplots package of R (https://cran.r-project.org/web/packages/gplots/index.html).

2.5. ceRNA interaction network construction and functional analysis

By integrated our previous published jejunum mRNA sequencing data (Wang et al., 2019a), we predicted and constructed the ceRNA (lncRNA-miRNA-mRNA) interaction network of jejunum from chicken exposed to NH_3 using Miranda (http://www.microrna.org/microrna/) and RNAhybrid software. According to the ceRNA hypothesis, we searched for potential MREs on the lncRNA and mRNA sequences. We predicted binding sequence sites in miRNAs, and overlapping of the same miRNA binding site on both lncRNAs and mRNA represented lncRNA-miRNA-mRNA interaction. Meanwhile, all mRNAs identified in the lncRNA-miRNA-mRNA interaction network were subject to Kyoto Encyclopedia of Genes and Genomes (KEGG) enrichment analysis (https://www.kegg.jp/) and Gene Ontology (GO) analysis (http://www.geneontology.org/). We used these functional analyses to assess the possible biological processes involved in target genes in ceRNA.

2.6. Cell culture, treatment, and transfection

We used chicken liver hepatocellular carcinoma (LMH) cells (purchased from ATCC, USA) to perform our in vitro tests. LMH cells (1×10^6 cells/mL) were cultured in 6-well plates (NUNC) in medium (DMEM) with 10 % fetal bovine serum (FBS, Gibco) in a 37 °C humidified atmosphere containing 5% CO_2. To investigate the pro-apoptosis effect of NH_3 in vitro, LMH cells were stimulated for 24 h with 3 mM and 6 mM NH_4Cl, respectively. Meanwhile, based on test requirements, we used chemically modified miR-205a mimic negative control (mimic-NC), miR-205a inhibitor negative control (inhibitor-NC), miR-205a mimic, inhibitor, lncRNA-107052630 siRNA (Guangzhou Ribo Biotechnology Co., Ltd) and pcDNA3.1$^+$-lncRNA-107052630 plasmid (Shanghai Sangon Biotech Co., Ltd) to conduct cell transfection assay. To study the role of miR-205a in the predicted crosstalk, LMH cells were divided into three groups: NC group (cells were transfected with mimic-NC and inhibitor-NC), Mimic group (cells were transfected with inhibitor-NC and miR-205a mimic) and Inhibitor group (cells were transfected with mimic-NC and miR-205a inhibitor). Similarly, to study the cellular role of lncRNA, LMH cells were divided into three groups: NC group (cells transfected with pcDNA3.1$^+$ plasmid and siNC), ovLnc group (cells were transfected with pcDNA3.1$^+$ plasmid-lncRNA-107052630 and siNC), and siLnc group (cells were transfected with pcDNA3.1$^+$ plasmid and si-lncRNA-107052630). The lncRNA-107052630 sequence was supplied in Table 1. The following concentrations of reagent used in the transfection experiment using Lipofectamine 2000 reagent (Invitrogen, USA) in Opti-MEM medium was miR-205a-mimic: 100 nM, mimic-NC: 100 nM, inhibitor-NC: 100 nM, miR-205a-inhibitor: 200 nM, and pcDNA3.1$^+$-lncRNA plasmid-107052630: 1 μg/mL. LncRNA-107052630 siRNA at 50 nM using the Lipofectamine RNAi MAX Reagent (Invitrogen, USA) according to the manufacturer's recommendation and our previous concentration validation. Meanwhile, to further verify the presence of ceRNA, LMH cells were grouped for a double-transfection test. For double overexpression transfection, compared with the positive control (LMH cells treated with 50 μM PAC-1 for 24 h (Selleck, China)), cells were transfected with miR-205a mimic or pcDNA3.1$^+$ plasmid-lncRNA-107052630 + miR-205a mimic, respectively. For double inhibition transfection, under NH_3 treatment, cells were transfected with miR-205a inhibitor or si-lncRNA-107052630 + miR-205a inhibitor compared to the negative control (cells treated with 50 μM z-VAD-fmk for 24 h (Selleck, China)).

2.7. Dual-luciferase reporter analysis

We first designed and constructed two tandem repeats of miR-205a response elements from wild G0S2 3′UTR (WT) or mutant G0S2 3′UTR (MUT). After annealing the oligonucleotides, the generated double-stranded nucleotide sequences were inserted into the pMIR-REPORT vector (Thermo Fisher) to product pMIR-G0S2 REPORT constructs (pMIR-G0S2-WT and pMIR-G0S2-MUT). The empty pMIR-REPORT vector was used as the negative control (pMIR-REPORT NC). Subsequently, we co-transfected miR-205a mimic and pMIR-G0S2-WT or MUT into LMH cells using Lipofectamine 2000 (Invitrogen),

Table 1
The sequence of lncRNA-107052630.

Sequence	GTTCACTGCAGCGGAGTTGGACTAGGTGACCTTTAAAGGTCCCTTCCAACTCAAACGATTCTGTGATTCTA TGATAACACAGAGTGAAGGTCATTTCGGTAGCCTCGGGTCAGGCACGTGGTGGGGTGAGCTGGAGGAGCTCCTGCC CAGCTCTGCACGATGCTGCGAGCTGGTGAGGGGCTGAGCTGACCTCGCTTCTCCTGCTGCTCGGCTGACTTACCGC TGCCCCGGGCCTTGCTAATGAAGGGCTTTAAGCAATTAAAAAAACAAGTAGCAGCACTGAGGTCCAGAGGGTGGAA AATTGCTGGATTTGTCTCTGCTCTGTGAAATTTGCTCAGGAGCAGGATGCTGCAGTGAGGCTTTCTGTGTTGTGCCATGGAGA GAGAAGGCAGTGCACTGTATCCCTCCCCAGTTTCCTGAACAATCAGGCAGTGATTTCTGTAACAACCCAGCATCTC CAAACGCTAGTGGTACAGAGCCAGGTTGTTTTTGCTTTATGCAGGGAAGTGCATTTGAAATCTTGCAATTATATGC ATGTTCAAATTGAACTCCTAGGCGTATGAGAAAACGGTGCTATTCTCCATTTCCCAGTAACTGATCAATGCTTTTTAACTCTC TTGGAATTGTGAATTTTGCTGCGGATTAACTGCTGCTATGAGACGCGGGGATGGAGCTTATGAAATTGATTTTTGACAGGAGGAAGT GGAAGGGTGAAACGCACATCTTCCTTTTCTAAAGTTGGATTGATCACGGCTGTTGTGAAGAACGGTAAGATGAAACAGGATGGTTTG CAATCTGCAGGTTTCCAGCCAGAGTCTGGCAACCTTGATGAAGAGTTTTCTGATTATAGGAGCTTTCTGCAAAAAGTAAGGGAATAA AAAGTAATTTATCACAGATTACTCTGCTACCATACCAGAAGTCTTTATATCAAATGAACAAATTGTACATACCCGCAGACAGTGGCAG GAAAACACCAGAAGGCCTTGAAACCCCACAATGACTTCTGTGTAATATACGCAGTTACCAGAGACAGACAACATACGGCCTCTGTAG AATCAGTTTTGCCATAAACTATACTCAAA GAGAATTTTTGAACTGTATCAAATACGCAACCGTTACCCAATTTGTTTTTGTTCTGTTTTTAAAGAAAGCCTTTCAAAAAAAAAACAT GCCTTCGTTAAACAGGAATTACTGAATCCCCACTCCTCGACTGCAGAAAACT TGGCTGACAAGTCAATTCTGGATGAAAAGCTGACGAGCACCGAGAAATGCTAATGTGGGAAAAATTCTATTCATTCTTCCTCTGCTAT AAGTCATCATCAGTGGCGCTGTTGAATGTTCATCTGTG ATTTAAGAAGGGAGAGGAAGAAAGAGCCGAGTACCTTCCTGGCTGCACGTTAAGCTCTCTGGAAGGAAATAGACAGAGCTCACGTCC CTGCATCCTTCAAGCAGGACATGAGGCTGTGAAGCACCCTTCTGGC TGAAGGAACATCTTGCCCCTGCTTATCCTGGGCTGGAGCTGGGTGCAGCACTCTTGTTGCGGTGGTCTGTTGGCACACAGCATTATCT GCCAGCAGTATGTGGCTCTCCCATCCCCAGGGAGGAAGGTCTTTACTCTTGCAGTGCCCCTGGTTGCCACTGAGATTTCA GCTTCTGGCAGAGCTGAGCTGTAATGCACCCAACACGGTACGGTTTTCCTACGCAATCACCAGCAGTGTGGCGTGGAGTCCCTTTGGT TGCACAAATGCTTTCCGTTGTGATGTACGCAGGTTGCA GTATGCCAGCATTGCAGTTAAACAGTTCGGAAGTGCAGTTTCATTAGCAAATTGTGGGATTTCTTCTCCAGCATGAACTTCTTG TCTCTGTCGTCTATGAAGAAAGCAACTTACAGAAATATTCCCATTGCTGAAAACGACACACCGAGGAAACGAATTCAAGAAGAAACA CCAGCTTCATTGCCAGGA TTGATTACAGGTCTATGCTATATGTTCTAGTGTCATATTAAATCCTGTATTAAAATTAAAGCATTGTTTTACA

according to the manufacturer's instruction. Luciferase activity was determined by the normalize result of Renilla luciferase activity relative to Firefly luciferase (Renilla LUC/Firefly LUC) using Dual-Luciferase Reporter Assay System (Promega).

Similar to the above steps, the preparation of luciferase construct of lncRNA-107052630-miR-205a binding sites was obtained using the sequence of lncRNA-107052630. The inserted sequence is presented in Table 2.

2.8. Morphology observation and quantitative analysis of apoptosis

We performed acridine orange/ethidium bromide (AO/EB) dual staining to observe cell apoptosis processes in LMH cells. In brief, after NH_4Cl treatment or transfection, cells (1×10^6 cells/mL) grown in 6-well plates were digested by trypsin and stained with AO/EB for 5 min. Nuclei of cells with intact membranes can be stained bright green by AO staining, while EB staining can only make cells emit orange-red fluorescence when their membranes are damaged. The apoptosis fluorescence image was visualized by employing fluorescence microscopy (Thermo Fisher Scientific, USA). Meanwhile, to quantitatively analyze the cell apoptosis under different treatments, an Annexin V-FITC/PI cell death detection kit was applied to regent-treated or transfected LMH cells according to the manufacturer's recommendations, and live cells were assessed by flow cytometry based on cells negative DAPI staining. For detection of apoptosis, we incubated cells with 500 μL of binding buff ;er containing 5 μL of PI and 5 μL of Annexin V-FITC for 30 min at room temperature in the dark. After incubation, the proportion of live, necrotic and apoptotic cells was identified by using flow cytometric analysis. The methods for calculating the rate of apoptosis were provided by the FlowJo 10.0 software as previously described (Wang et al., 2009; Li et al., 2020).

2.9. Real-time quantitative PCR analysis (qRT-PCR)

To identify the reliably of RNA sequencing results and prove the existence of the ceRNA relationship, we selected the genes involved in ceRNA network-regulated apoptosis for validation using qRT-PCR. Total RNA and total miRNA from chicken jejunum exposed to NH_3 (n = 3) and LMH cells after NH_4Cl treatment or transfection (n = 3) were extracted with Trizol Reagent (Invitrogen, Carlsbad, CA, USA)

Table 2
lncRNA- 107052630 and G0S2 wild type/mutant type sequences.

3′UTR	Forward (5′-3′)	Reverse (5′-3′)
G0S2-pMIR-REPORT-WT	AGCTTCAGCGATGGTGGT TCCAGTGAGGAGGATGAAGGTTTGGCTG AATGTGGAGGCTGCGAAGAGCT	CTTCGCAGCCTCCACATTCAGCCAA ACCTTCATCCTCCTCACTGG AACCACCATCGCTGA
G0S2-pMIR-REPORT-MT	AGCTTCAGCGATGGTGGTTCCAGTGAGGACGAC GGATGTTTGGCTGAATGTGGAGGCTGCGAAGAGCT	CTTCGCAGCCTCCACATTCAGC CAAACATCCGTCGTCCTCACTGG AACCACCATCGCTGA
lncRNA-107052630-pMIR-REPORT-WT	AGCTTGGTCAGGCACGTGGTGGGGTGAGCTGGA GGAGCTCCTGCCCAGCTCTGCACGATGCTGAGCT	CAGCATCGTGCAGAGCTGGGCAGGAG CTCCTCCAGCTCACCCC ACCACGTGCCTGACCA
lncRNA-107052630-pMIR-REPORT-MT	AGCTTGGTCAGGCACGTGGTGGGG TGAGCCGGTAGAGCTCCTGCCCAGCTCTGCACGATGCTGAGCT	CAGCATCGTGCAGAGCTGGGCAGGA GCTCTACCGGCTCACCCC ACCACGTGCCTGACCA

Table 3
Gene-special primers used in the real-time quantitative reverse transcription PCR.

Gene	Forward Primer (5′→ 3′)	Reverse Primer (5′→ 3′)
G0S2	GTTCTTCGGCGTGGTCATCGG	GTTCTTCGGCGTGGTCATCGG
Bcl2	ATCGTCGCCTTCTTCGAGTT	ATCCCATCCTCCGTTGTTCT
Bax	TCCATTCAGGTTCTCTTGACC	GCCAAACATCCAAACACAGA
Cas9	ATTCCTTTCCAGGCTCCATC	CACTCACCTTGTCCCTCCAG
Cas3	CATCTGCATCCGTGCCTGA	CTCTCGGCTGTGGTGGTGAA
CytC	TGGACCTGAAGCGACCTCTGC	CATCACATCTTCACGACGGTAGGC
LOC107052630	ACTCTTGTTGCGGTGGTCTGTTG	CACACTGCTGGTGATTGCGTAGG
β-actin	CCCATCTATGAGGGCTACGCT	TCCTTGATGTCACGGACGATT
miR-205a	TCCTTCATTCCACCGGAGTCTG	
U6	CACGCAAATTCGTGAAGCGCCTTA	

according the manufacturer's standards. First-strand cDNA was synthesized using a BioRT Master HiSensi cDNA First Strand Synthesis kit (Bioer Technology Co. Ltd., Hangzhou, China) or miRcute microRNA First-Strand cDNA Synthesis Kit (Tiangen Biotech Co. Ltd., Beijing) according to the manufacturer's instructions. Primers for the detection of miR-205a, lnc-107052630, target gene G0S2 and mitochondrial apoptosis signaling molecules (Bcl2, Bax, Cas9, Cas3, CytC) are presented in Table 3. U6 and β-actin were used as internal references. qRT-PCR was performed using LightCycler® 480 II Detection System (Roche, Switzerland). In the melting curve analysis, each PCR product showed only one peak. Considering gene-specific efficiency, the relative abundance of mRNA was computed via the $2^{-\Delta\Delta Ct}$ method and normalized to the mean expression.

2.10. Western blot analysis

LMH cells were seeded in 6-well plates (1×10^6 cells/mL) following NH4Cl treatment or transfection. Then, jejunum tissue from NH_3-exposed chicken and cells were harvested, rinsed with 1 × PBS and lysed in ice-cold RIPA lysis buffer containing 1 mM PMSF. Supernatants were harvested by centrifugation at 4 °C and 12,000 × g. We used bicinchoninic acid assay to determine the concentration of protein. Total protein was exacted by RIPA (Beyotime Biotechnology) supplemented with 1% PMSF and subjected to 12 % SDS-polyacrylamide gel electrophoresis. After transferring the separated protein to nitrocellulose membranes, we blocked the NC membranes in 5% skim milk powder for 2 h at 37 ℃. Then membranes were washed with TBST 3 times and incubated with primary antibodies at 4℃ overnight. The antibodies used in this study include G0S2 (1:1000 Abcam, Cambridge, UK), Caspase3 (1:500, produced by our lab), cleaved Caspase3 (1:1000, Wanlei, Shenyang, CN), Bcl2 (1:1000, Wanlei, Shenyang, CN), CytC (1:1000, CST, Boston, US), and β-actin (1:5000, Abclonal, China), followed by a HRP-conjugated goat anti-rabbit IgG secondary antibody (1:5000, Santa Cruz, USA). Image J software (National Institutes of Health) was used for densitometry. β-actin was used to verify equal protein loading.

2.11. Immunofluorescence staining

We cultured LMH cells in 24-well plates for double-transfection tests to complete the experiment of immunofluorescence. After 24-h transfection, cells of each groups were fixed in paraformaldehyde (solution 4% in PBS) for 30 min and then rinsed with PBS 3 times (5 min each). Next, the cells were permeabilized in 0.1 % Triton X-100 for 15 min and blocked with 5% BSA for 1 h. After overnight incubation at 4 ˚C with anti-G0S2 antibody (1:50, Abcam, Cambridge, UK), cells were treated with Dylight 594-conjugated AffiniPure Goat Anti-rabbit IgG (1:500, Bioworld, USA) and incubated at room temperature without light for 1 h. DAPI staining (Beyotime, China) was used to visualize cell nuclei. The images of immunofluorescence were obtained by fluorescence microscopy (Thermo Fisher Scientific, USA) and the area labeled with anti-G0S2 displayed red. Positive areas in cells were measured using ImageJ software (National Institutes of Health).

2.12. Statistic

Student's $t-$test was performed to assess the effect of jejunum differentiation between the C group and the NH3 exposed group using GraphPad Prism 5 (San Diego, CA, USA). Variance in different groups in vitro test was assessed by using one−way ANOVA. Quantitative data are presented as the mean ± SD. For in vivo tests, samples with star (*) represent statistically significant differences ($P < 0.05$). For in vitro tests, samples with different superscript letters represent statistically significant differences ($P < 0.05$).

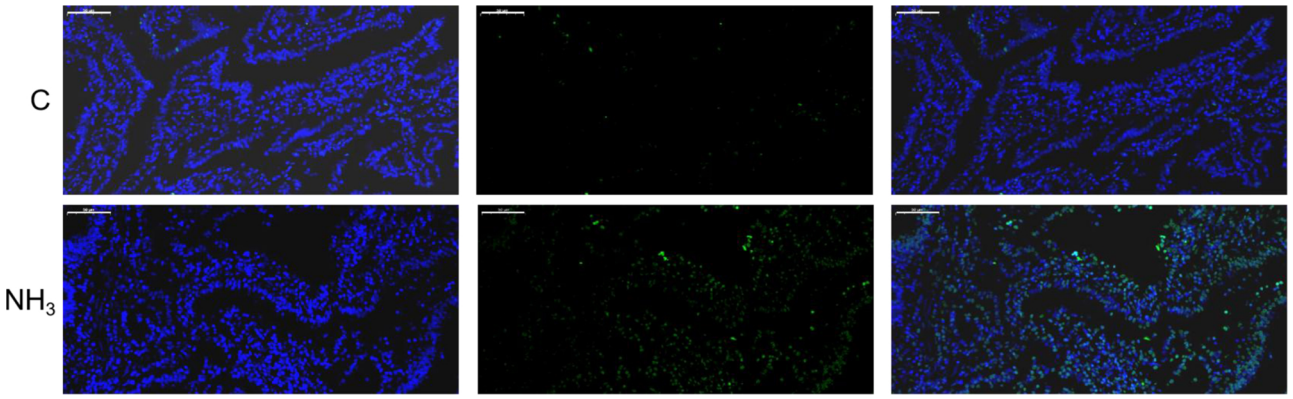

Fig. 1. Effect of NH_3 exposure on apoptosis of chicken jejunum. TUNEL staining analysis of apoptosis in jejunum of chicken from C group and NH_3 exposed group. DAPI (blue): a cell nucleus marker. TUNEL (green): terminal dUTP nick-end labeling, a marker for apoptosis. Scale bars are 50 μm. (For interpretation of the references to colour in this figure legend, the reader is referred to the web version of this article).

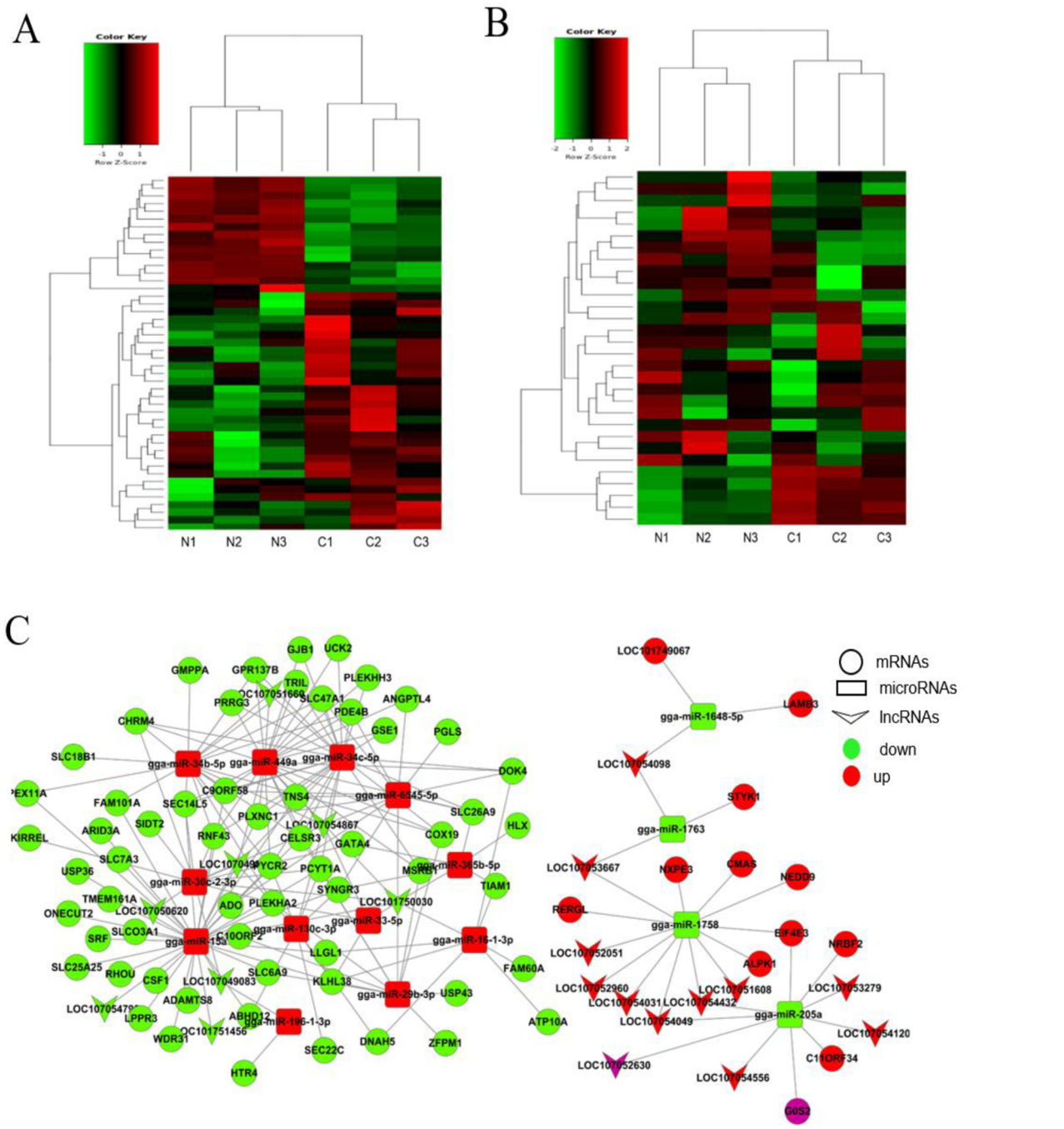

Fig. 2. A: Heat map with intuitive reflection of the 46 different expressed lncRNAs in the jejunum of chicken between C group and NH_3 group. represented that gene expression levels increased from left to right (FC > 1.5, FDR < 0.05). B: Heat map with intuitive reflection of the 30 different expressed miRNAs in the jejunum of chicken between C group and NH_3 group (FC > 1.5, FDR < 0.05). represented that gene expression levels increased from left to right. C: LncRNA-miRNA-gene interaction network consists of 20 lncRNAs (triangular cones), 16 miRNAs (squares), and 74 mRNAs (circles). Red color means up-regulated RNAs and green color means down-regulated RNAs. (For interpretation of the references to colour in this figure legend, the reader is referred to the web version of this article).

3. Results

3.1. Histologic observation

The histological changes in jejunal cells from the C group and the NH_3 exposed group were observed using TUNEL staining. Apoptotic cells can be stained green by specific fluorescent dyes in TUNEL assay. As shown in Fig. 1, jejunal cells of control group exhibted normal living conditions, only a few individual cells undergone apoptosis and were stained green. However, after NH_3 exposure, a large number of jejunal cells showed green fluorescence, indicating NH_3 exposure caused apoptotic programmed death of cells in chicken jejunum.

3.2. RNA-sequencing and construction of ceRNA interaction network

The data output quality and the classification of mapped reads in miRNA profiles of jejunum from NH_3-exposed chicken was shown in Table. S1, and similar information of lncRNA profiles was reported in our previous study (Wang et al., 2019a). In total 46 differentially expressed lncRNAs (Fig. 2A) and 30 differentially expressed miRNAs

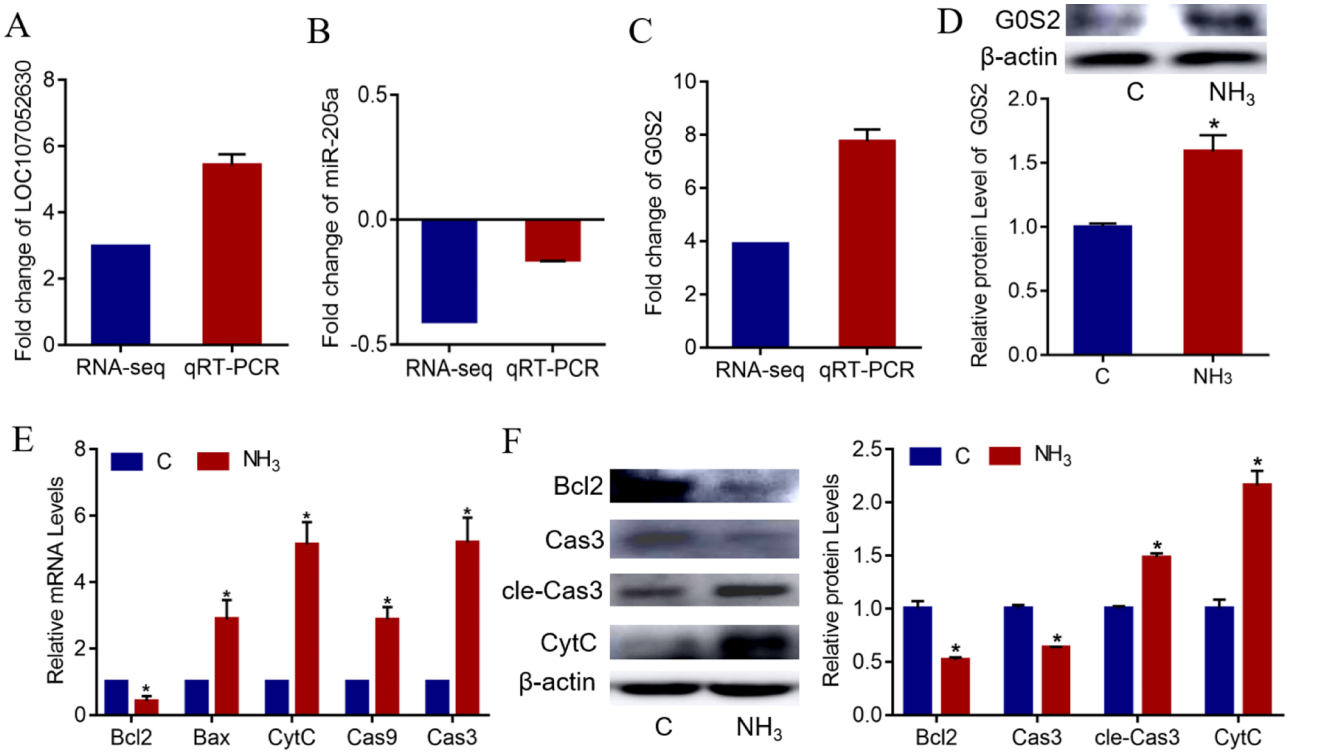

Fig. 3. Discovery of lncRNA-107052630/miRNA-205a/G0S2 crosstalk in jejunum after NH_3 exposure. A: qRT-PCR of lncRNA-107052630 compared with RNA-seq in jejunum exposed to NH_3. B: qRT-PCR of miR-205a compared with RNA-seq in jejunum exposed to NH_3. C: qRT-PCR of G0S2 compared with RNA-seq in jejunum exposed to NH_3. D: The protein expression of G0S2 detected by western blot. E and F were the results of mitochondrial apoptosis pathway genes expression at mRNA and protein levels. Data are shown as the mean ± SD values. * shows the significant difference, $p < 0.05$ by student's *t*-test.

(Fig. 2B) were identified with FC > 1.5; FDR < 0.05 as cut off (Table. S4, S5). Our previous study showed the dysregulated mRNA profile between control and NH_3-exposed broiler jejunum, and 677 differentially expressed mRNAs were identified (Wang et al., 2019a). LncRNAs and protein encoding RNAs (mRNAs) can competitively bind to the common interaction site located at miRNAs and regulate the expression of each other. Here, using Miranda and RNAhybrid software, we predicted and constructed a lncRNA-miRNA-mRNA crosstalk network (ceRNA network) in jejunum form chickens under NH_3 exposure. This ceRNA network contains 539 pairs of lncRNA-miRNA-mRNA single crosstalks, including 74 mRNAs, 16 miRNAs and 20 lncRNAs (Fig. 2C).

3.3. Discovery of lncRNA-107052630/miRNA-205a/G0S2 crosstalk in vivo

RNA-seq revealed that 15 lncRNAs and 5 miRNAs were downregulated, and 31 lncRNAs and 25 miRNAs were upregulated in jejunum of control and NH_3-exposed broilers, respectively (Fig. 2A, B). LncRNA-seq identified a lncRNA (lncRNA-107052630) that was significantly upregulated to about 3.5 folds in the jejunum of NH_3-exposure group and the expression trend was confirmed by qRT-PCR (Fig. 3A). The ceRNA prediction network showed that lncRNA-107052630 and miR-205a exist functional element by bioinformatics analysis. RNA-seq and qRT-PCR identified that miR-205a was significantly decreased in the NH_3-exposure group compared to the control group (Fig. 3B). Meanwhile, the coding genes identified in the ceRNA network were enriched using Pathway analysis and GO analysis (Table. S6, 7). Notably, according to GO analysis, we found that the G0S2 gene was enriched in the extrinsic apoptotic signaling pathway. G0S2 can promote apoptosis by antagonizing the anti-apoptosis factor Bcl2 and is also the predicted target gene of miR-205a. Here, mRNA and protein levels displayed that G0S2 and mitochondrial apoptosis pathway genes (Bax, CytC, Cas3, Cas9) were activated ($P < 0.05$), and Bcl2 expression was inhibited (Fig. 3C–F). Thus, we hypothesized that the lncRNA-107052630/miRNA-205a/G0S2 axis may play an important role in NH_3-induced intestinal apoptosis.

3.4. Verification of lncRNA-107052630/miRNA-205a/G0S2 crosstalk

To prove our hypothesis, we used dual-luciferase reporter gene assays to validate that miR-205a directly interacts with lncRNA-107052630 in vitro. Transfection of miR-205a mimics into LMH cells modulated luciferase activity indicating that miR-205a interacted with the binding site of wild type of lncRNA-107052630 transferred into cells ($P < 0.05$). However, the miR-205a mimics could not decreased the luciferase activity driven by the binding site of mutant type of lncRNA-107052630 (Fig. 4A) ($P < 0.05$). In addition, dual-luciferase reporter gene assay result also showed that miR-205a can directly interact with G0S2 (Fig. 4B). Subsequently, we transfected pcDNA3.1$^+$-lncRNA-107052630 overexpression plasmid and si-lncRNA-107052630 into LMH cells, to generate the ovLnc group and siLnc group, respectively. The expression of miR-205a decreased in response to lncRNA-107052630 overexpression and increased in response to lncRNA-107052630 knockdown (Fig. 4C) ($P < 0.05$). Changes of G0S2 expression were consistent with changes in expression of lncRNA-107052630 (Fig. 4D, E). Additionally, overexpression of miR-205a simultaneously reduced the expression of lncRNA-107052630 and G0S2 ($P < 0.05$), and miR-205a knockdown could simultaneously induce the expression of lncRNA-107052630 and G0S2 (Fig. 4F–H). These results indicated that lncRNA-107052630 indeed protected G0S2 expression by functioning as a molecular sponge for miR-205a that specifically inhibits G0S2 in the jejunum from chickens exposed to NH_3.

3.5. Effect of lncRNA-107052630 and miR-205a on apoptosis in vitro

We further estimated the effect of lncRNA-107052630 on apoptosis

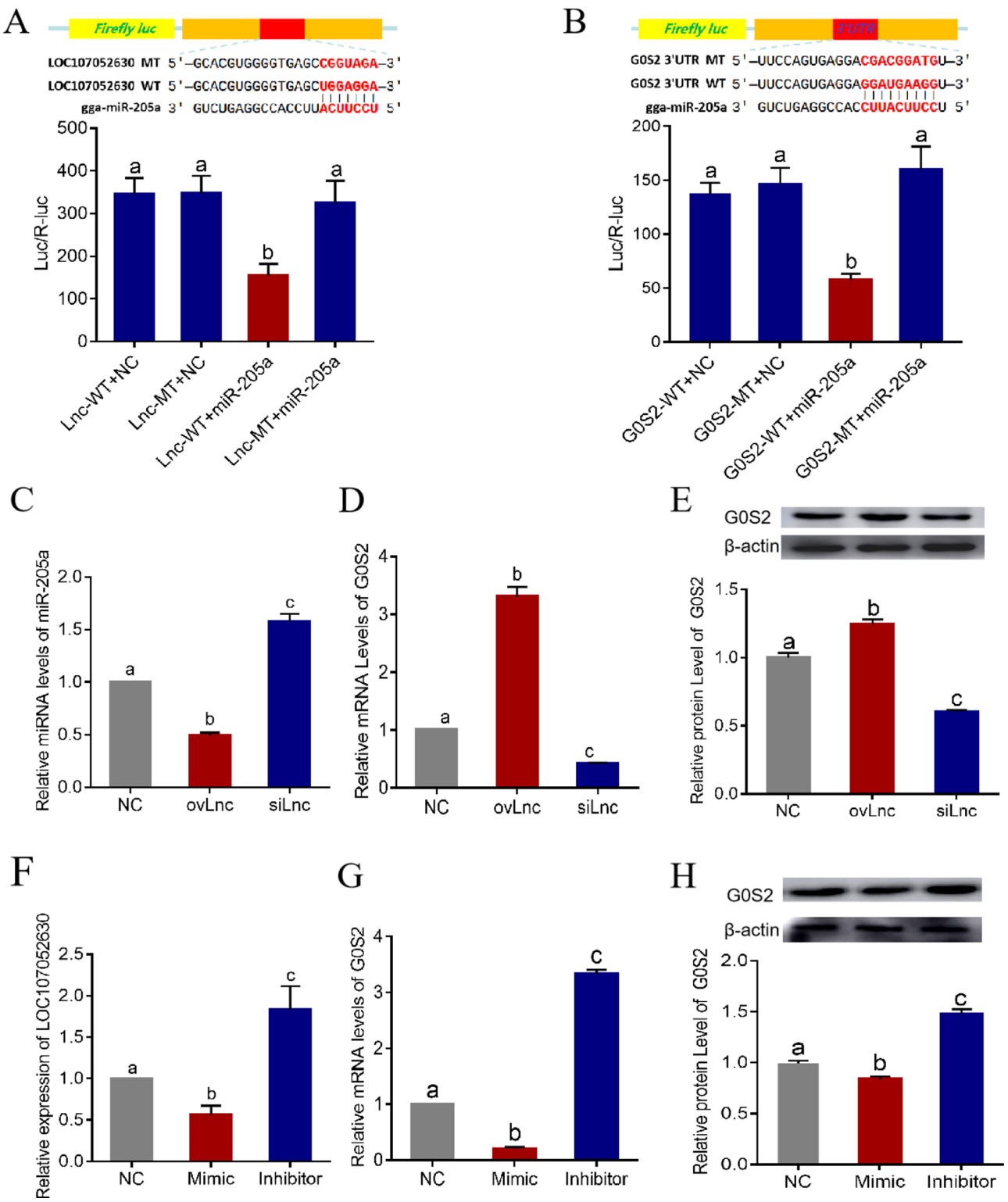

Fig. 4. Verification of lncRNA-107052630/miRNA-205a/G0S2 crosstalk. A: Correlation between lncRNA-107052630 and miR-205a in luciferase reporter gene assay results. pMIR-lncRNA-107052630-WT plasmids was mutated in the miRNA target sites, and designated as pMIR-lncRNA-107052630-MT. miR-205a mimic inhibits lncRNA-107052630-WT expression but not mutant lncRNA-107052630-MT expression. B: Correlation between G0S2 and miR-205a in luciferase reporter gene assay results. pMIR-G0S2-WT plasmids was mutated in the miRNA target sites, and designated as pMIR-G0S2-MT. miR-205a mimic inhibits G0S2-WT expression but not mutant G0S2-MT expression. C: The expression of miR-205a in NC group (LMH cells transfected with pcDNA3.1$^+$ plasmid and siNC), ovLnc group (cells were transfected with plasmid of pcDNA3.1$^+$-lncRNA-107052630 and siNC), and siLnc group (cells were transfected with plasmid of pcDNA3.1$^+$ and Si-lncRNA-107052630). D, E: The mRNA and protein expressions of G0S2 in NC, ovLnc, and siLnc group. F: The expression of lncRNA-107052630 in NC group (LMH cells were transfected with mimic-NC and inhibitor-NC), Mimic group (cells were transfected with inhibitor-NC and miR-205a mimic), and Inhibitor group (cells were transfected with mimic-NC and miR-205a inhibitor). G, H: The mRNA and protein expressions of G0S2 in NC, Mimic, and Inhibitor group. Data are shown as the mean ± SD values. Bars that do not share the same letters are significantly different ($p < 0.05$) from each other.

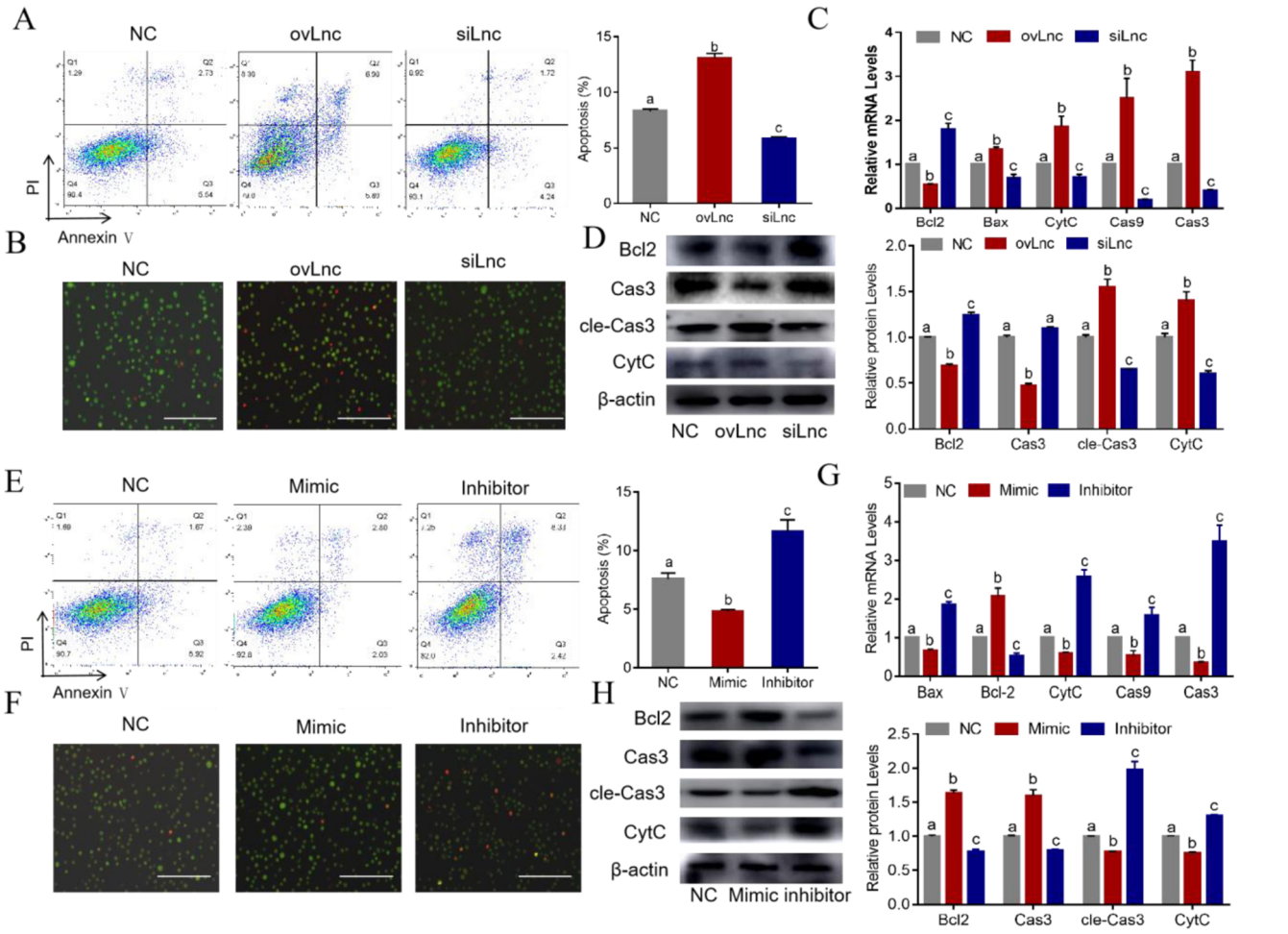

Fig. 5. miR-205a and lncRNA-107052630 were involved in apoptosis in vitro. A: Cell viabilities and apoptosis rate of LMH cells in NC, ovLnc, and siLnc group detected by flow cytometry analysis. B: Detection results of AO/EB staining of LMH cells in NC, ovLnc, and siLnc group, normal cells (green), and apoptosis cells (bright orange). Scale bars are 200 μm. C, D: The mRNA and protein expressions of G0S2 in LMH cells of NC, ovLnc, and siLnc group. E: Cell viabilities and apoptosis rate of LMH cells in NC, Mimic, and Inhibitor group detected by flow cytometry analysis. F: Detection results of AO/EB staining of LMH cells in NC, Mimic, and Inhibitor group. Scale bars are 200 μm. G, H: The mRNA and protein expressions of G0S2 of LMH cells in NC, Mimic, and Inhibitor group. Data are shown as the mean ± SD values. Bars that do not share the same letters are significantly different ($p < 0.05$) from each other. (For interpretation of the references to colour in this figure legend, the reader is referred to the web version of this article).

in vitro by performing flow cytometry on LMH cells. The apoptosis rates in the NC, ovLnc and siLnc groups were 8.27 %, 12.7 % and 5.96 %, respectively (Fig. 5A). AO/EB staining revealed more apoptotic cells that appeared range with EB staining in the ovLnc group than in NC (Fig. 5B), which indicated that lncRNA-107052630 increased the occurrence of apoptosis in LMH cells. Meanwhile, the results of RT-PCR and western blot showed that lncRNA-107052630 overexpression inhibited Bcl2 expression, promoted the activation of Cas3 and exacerbated the transition from Cas3 to apoptotic executor cleaved Cas3 compared with the NC group (Fig. 5C, D) ($P < 0.05$). Oppositely, lncRNA-107052630 knockdown increased Bcl2 expression and attenuated the generation of cleaved Cas3 ($P < 0.05$). The results showed that lncRNA-107052630 can activate mitochondrial apoptotic pathway in LMH cells.

To estimate the effect of miR-205a on apoptosis, we transfected LMH cells with miRNA NC, miR-205a mimics and miR-205a inhibitor. Flow cytometry analysis revealed that the apoptosis rates in NC, mimic and inhibitor groups were 7.59 %, 4.76 % and 11.60 % (Fig. 5E). AO/EB staining showed more apoptotic cells were stained with orange by EB after miR-205a inhibitor transfection (Fig. 5F). Detection of expression changes of mitochondrial apoptotic pathway molecules confirmed that increased miR-205a levels obviously increased Bcl2 expression and inhibited the activation of Cas3 ($P < 0.05$), whereas decreased miR-205a levels promoted the generation of cleaved Cas3 (Fig. 5G, H). These results showed that miR-205a can inhibit apoptosis and mitochondrial apoptotic pathway activation in LMH cells.

3.6. Detection of the effect of NH_4Cl on apoptosis in vitro

We simulated NH_3 exposure by stimulating cultured LMH cells with NH_4Cl in an in vitro environment. Flow cytometric analysis showed that with the increase of NH_4Cl stimulation concentration, the percentage of cell death also increased. Compared with the apoptotic rate in control group, the apoptosis rate of the cells was increased by 41.21 % and 146.13 % under the stimulation of 3 mM and 6 mM NH_4Cl, respectively (Fig. 6A). AO/EB staining showed that NH_4Cl caused more cells appeared bright orange, indicating apoptosis occurrence (Fig. 6B). Meanwhile, consistent with detection results of jejunum from chickens under NH_3 exposure, the expression levels of lncRNA-107052630 and miR-205a were gradually increased and decreased by NH_4Cl, respectively (Fig. 6C). Quantitative analysis of mRNA and protein showed that NH4Cl activated G0S2 regulated mitochondrial apoptosis pathway in LMH cells (Fig.6D, E). These results indicated NH_4Cl can induce apoptosis, and lncRNA-107052630/miR-205a/G0S2 ceRNA crosstalk may be universal in chicken tissues.

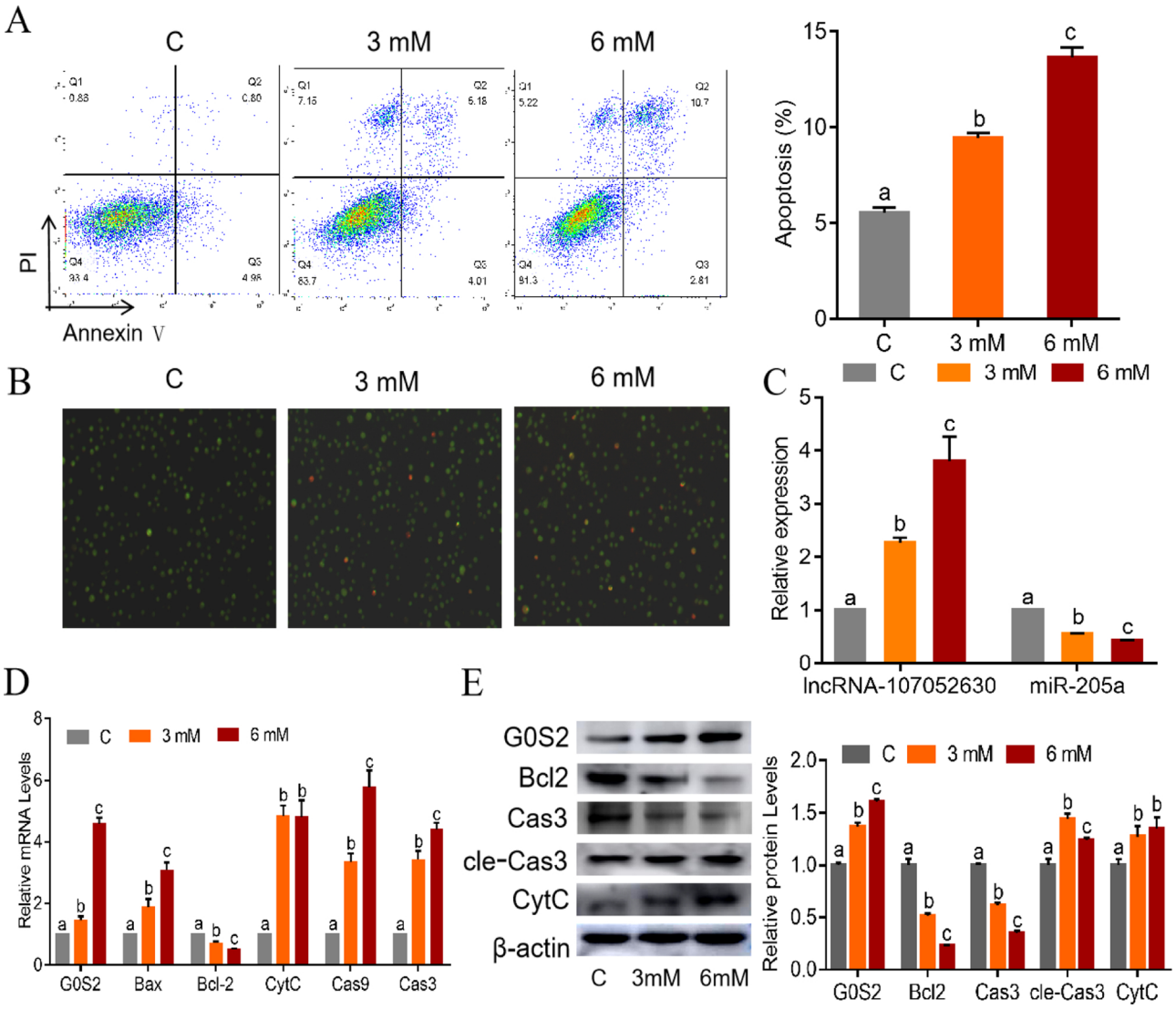

Fig. 6. LncRNA-107052630/miR-205a/G0S2 crosstalk exists in LMH cells stimulated with NH_4Cl. LMH cells were treated with 3 mM NH_4Cl and 6 mM NH_4Cl for 24 h, respectively. A: Cell viabilities and apoptosis rate in LMH cells detected by flow cytometry analysis. B: Detection results of AO/EB staining in LMH cells, normal cells (green), and apoptosis cells (bright orange). C: The expression of lnRNA-107052630 and miR-205a of LMH cells. D, E: The mRNA and protein expressions of G0S2 and mitochondrial pathway related genes in LMH cells. Data are shown as the mean ± SD values. Bars that do not share the same letters are significantly different ($p < 0.05$) from each other. (For interpretation of the references to colour in this figure legend, the reader is referred to the web version of this article).

3.7. lncRNA-107052630 modulates G0S2-induced apoptosis through competitive binding of miR-205a

To further demonstrate that lncRNA-107052630 and miR-205a are important factors involved in apoptosis mediated by G0S2 via combination intervention rather than independent effects, we performed co-expression and co-knockdown experiments on these two non-coding RNAs in LMH cells. Flow cytometry showed the apoptosis ratio of each group, and immunofluorescence was used to analyze the expression of G0S2. As shown in Fig. 7A–D, compared to the apoptosis ratio and G0S2 expression in the positive control group (PAC-1 group: cells were treated with caspase activator (PAC-1), which can bypass G0S2 intervention and directly initiate apoptosis by activating Cas3), the PAC-1 + miR-205a mimic group exhibited reduced apoptosis rate and G0S2 fluorescence intensity, and this inhibitory effect can be offset by transfection of a lncRNA-107052630-overexpression plasmid ($P < 0.05$). In addition, under NH_4Cl stimulation, cells treated with Z-VAD-fmk (a apoptosis inhibitor that diretly inhibits the caspase activity) showed decreased apoptosis rate, while G0S2 expression was not affected, and was still comparable to that of NH_4Cl. Corresponding to the above results, after transfection of miR-205a inhibitor, the inhibited apoptosis rate was restored and the G0S2 fluorescence intensity was further strengthened, while lncRNA-107052630 knockdown antagonized the effect of miR-205a inhibitor on apoptosis, and decreased the expression of G0S2 again. The changes in Cas3 and cleaved Cas3 protein levels are shown in Fig. S1. These results clearly demonstrate that lncRNA-107052630 as ceRNA for miR-205a regulates the expression of G0S2 and then activates the mitochondrial apoptosis pathway (Fig. 7E).

4. Discussion

In air pollution, the emergence of excessive apoptosis in tissue has been gradually considered to be one of the toxicological markers of harmful gases (Tuzlak et al., 2016; Wang et al., 2019b). Additionally, co-exposure of $PM_{2.5}$, sulfur dioxide (SO_2) and nitrogen dioxide (NO_2) caused neuronal apoptosis in the mouse cortex, thus repressing the ratio of brain to body weight, deteriorating spatial learning and memory, and resulting in abnormal neurobehavior (Ku et al., 2016). Although NH_3 is a gas pollutant mainly produced from agricultural production, it has been underestimated in the secondary inorganic aerosols formation,

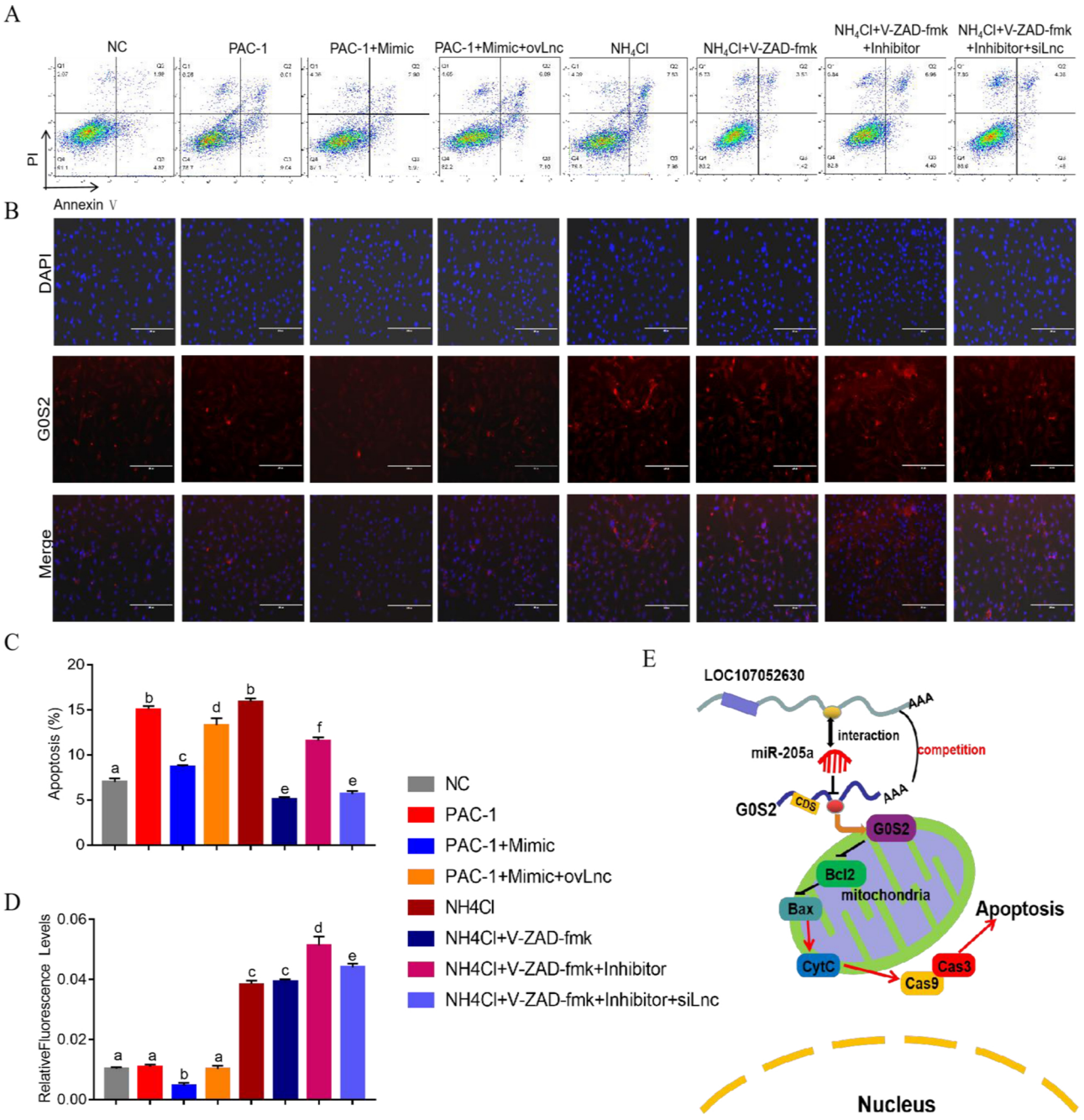

Fig. 7. lncRNA-107052630 modulates G0S2-induced apoptosis through competitive binding of miR-205a. Cell viabilities and apoptosis rate of LMH cells in PAC-1 group (50 μM PAC-1 added based on NC group), PAC-1 + Mimic group (PAC-1 + miR-205a mimic + plasmid of pcDNA3.1 +), PAC-1 + Mimic + ovLnc group (PAC-1 + miR-205a mimic + plasmid of pcDNA3.1 + -lncRNA-107052630), NH_4Cl group (6 mM NH_4Cl + Inhibitor NC + siNC), NH4Cl group (6 mM NH4Cl + Inhibitor-NC + siNC), NH4Cl + V-ZAD-fmk group (NH_4Cl + V-ZAD-fmk + Inhibitor-NC + siNC), NH4Cl + V-ZAD-fmk + Inhibitor group (NH_4Cl + V-ZAD-fmk + miR-205a inhibitor + siNC), and NH_4Cl + V-ZAD-fmk + Inhibitor + siLnc group (NH_4Cl + V-ZAD-fmk + miR-205a inhibitor + silncRNA-107052630). B: The G0S2 expression of cells observed through immunofluorescence staining, DAPI (blue): a cell nucleus marker. G0S2 (red). Scale bars are 200 μm. C: The diagram of lncRNA-107052630/miR-205a/G0S2 ceRNA mechanism. (For interpretation of the references to colour in this figure legend, the reader is referred to the web version of this article).

which is the main component of $PM_{2.5}$ concentrations in urban environment (Wu et al., 2016; Wang et al., 2017). Most previous studies on NH_3 have focused on the damage to the respiratory tract and immune system while neglecting the effect and mechanism of NH_3 on digestive system (Wang et al., 2019c; Kathyayani et al., 2019). In this study, we first confirmed that NH_3 can cause apoptosis in broiler jejunum cells based on morphological observation. Meanwhile, we identified that a lncRNA-associated-ceRNA network (lncRNA-107052630/miR-205a/G0S2 axis) was involved in NH_3-induced intestinal apoptosis via transcriptomics analysis and ceRNA networks prediction.

Given the regulation to mRNAs and sensitivity to external stimulation, non-coding RNAs have been widely regarded as biomarkers in environmental health risk assessment (Wang and Tang, 2019; Duan et al., 2017). Using transcriptomics analysis, the mechanism of different biological processes can be studied according to the non-coding RNAs that are abnormally expressed in organisms under environmental stress. For example, by analyzing the blood of healthy steel factory workers

through transcriptology, it was found that 17 miRNAs related with adverse cardiovascular and metabolic effects could be significantly changed by continuous exposure to particulate metallic components (Pavanello et al., 2016). Moreover, lncRNA-sequencing results showed that high concentrations of smoky coal combustion emissions were associated with non-small cell lung cancer through overexpression of lncRNA CAR intergenic 10 (Wei et al., 2016). In the present study, miRNA-sequencing and lncRNA-sequencing analysis of chicken jejunum from the NH_3 group and C group were employed, and we screened 30 different expressed miRNAs (25 upregulated miRNAs and 5 downregulated miRNAs) and 46 different expressed lncRNAs (31 upregulated lncRNAs and 15 downregulated lncRNAs), respectively, which indicated that NH_3 exposure could change the expression levels of non-coding RNAs in jejunum and some of these abnormally expressed miRNAs and lncRNAs may be involved in the the NH_3-induced apoptosis.

Recent reports identify a new complex interactivity among diverse RNA species, called ceRNA crosstalk (Yang et al., 2019; Li et al., 2017). The ceRNA hypothesis believes that lncRNAs or cirRNAs in the body can act as competitors of mRNAs, seize the binding site on the miRNAs that target mRNAs, and thereby alter mRNA expression and translation (Xu et al., 2015). The upregulated ceRNA can reduce the inhibitory effect of miRNA on mRNA and increase the expression of mRNA by competitively binding to the site sequence on miRNA (Le et al., 2017). Many researches have confirmed the regulatory role of ceRNA on apoptosis under conditions of external stimulation. LncRNA H19, which acts as a ceRNA of miR-148b, promoted proliferation and suppressed apoptosis by modifying the WNT/β-catenin signaling pathway in vascular smooth muscle cells stimulated by ox-LDL (Zhang et al., 2018). In the model of lipopolysaccharide-induced lung injury, lncRNA SNHG 16 was highly expressed, effectively binded to miR-146a-5p and restored CCL 5 expression, thereby promoting the inflammatory response and apoptosis (Zhou et al., 2019). However, only a several of studies proved that the crucial role of the ceRNA theory in study of the injury mechanism of air pollution. For example, cirRNAs mediated ceRNA network was involved in the response of chronic obstructive pulmonary disease to cigarette extract by affecting some genes involved in pentose phosphate pathway, ATP binding cassette transporters and cancer-related pathway via gene sequencing and analysis (Zeng et al., 2019). Especially, our latest study identified lncRNA-107053293 as a key regulator of necroptosis that acts on miR-148a-3p/FAF1 signaling and serves as a predictor of respiratory tract exposed to NH_3 (Wang et al., 2019c). In this study, using bioinformatics analysis, we screened and matched the sequences of differentially expressed lncRNAs, miRNAs and previously obtained dysregulated mRNAs, and constructed a ceRNA interaction network in the jejunum from chickens exposed to NH_3. Importantly, based on the functional analysis of target genes in the ceRNA network, we surprisingly found the up-regulated lncRNA-107052630 may function as ceRNA for miR-205a to control expression abundance of G0S2, a novel gene located in mitochondria that antagonizes the anti-apoptotic effects of Bcl2 under inflammatory conditions, thus inducing cell death (Welch et al., 2009). Additionally, it has been reported that G0S2, as a transcriptional activator in response to renal inflammation, aggravated the degree of apoptosis and chronic kidney disease (Matsunaga et al., 2016). As one of the main types of apoptosis, the mitochondrial apoptotic pathway is regulated by Bcl2 family proteins that can change the permeability of mitochondrial membrane, induce the release of CytC from mitochondria into the cytoplasm, and ultimately activate the caspase cascade (Cas9 and Cas3) to mediate apoptosis. Accordingly, we examined the expression of mitochondrial apoptosis pathway related genes in jejunum. The results showed that the pro-apoptotic genes (Bax, CytC, Cas9, and Cas3) were activated, and the anti-apoptotic gene Bcl-2 was inhibited by NH_3 exposure. These fingdingswere consistent with the conclusion that exposure to mountaintop removal mining particulate matter (PM MTM) increased the incidence of cardiovascular disease in the surrounding population by disrupting mitochondrial function and activating Cas3 and Cas9 (Nichols et al., 2015). Wang's research has chosen LMH cell line to validate ceRNA targeting relationship in chicken trachea exposed to NH_3 (Wang et al., 2019c). Chen et al. proved the presence of FOS/IL8 signaling regulated by H_2S in LMH cell in vitro (Chen et al., 2019b). Here, we also used LMH cells to determine whether the ceRNA network regulated apoptosis. Dual luciferase report analysis confirmed the existence of MREs in lncRNA-107052630/miR-205a/G0S2. Meanwhile, consistent with the results from jejunum in NH_3-exposed chicken, both lncRNA-107052630 overexpression and miR-205a inhibition promoted G0S2 expression, activated the mitochondrial apoptosis pathway and aggravate the emergence of apoptosis. Contrarily, G0S2-meidated cell death was relieved by lncRNA-107052630 inhibition and miR-205a overexpression. Further co-expression experiments confirm once again the existence of this ceRNA relationship. It was found that miR-205a alleviated PAC-1-induced apoptosis, which can be restored by increase of lncRNA-107052630. While under NH_4Cl stimulation, the miR-205a inhibitor promoted the rate of apoptosis inhibited by V-ZAD-FMK, which can be decreased by lncRNA-107052630 inhibition. Therefore, we have reasons to believe that lncRNA-107052630 and miR-205a are interdependent in the process of apoptosis regulated by G0S2.

In conclusion, we found that NH_3 exposure caused apoptotic-death of jejunal cells in chicken. RNA sequencing and ceRNA network analysis identified that in the differentially expressed non-coding RNAs under NH_3 exposure, lncRNA-107052630 functions as the ceRNA of miR-205a to positively modulate jejunal cells and LMH cells apoptosis caused by NH_3. G0S2, a target gene driven by miR-205a, effectively activating apoptosis by interacting with the key mitochondrial pathway gene Bcl2 and decreasing its expression. Due to the increasingly levels of NH_3 in air pollution, the results obtained in this study are valuable for understanding the intestinal toxicity of NH_3, and provide a theoretical basis and reference for studies on the role of non-coding RNAs in the cellular response to air pollution.

CRediT authorship contribution statement

Wang Shengchen: Conceptualization, Methodology, Software, Investigation, Writing - original draft. **Wang Wei:** Validation, Formal analysis, Visualization, Software. **Li Xiaojing:** Validation, Formal analysis, Visualization. **Zhao Xia:** Resources, Writing - review & editing, Supervision, Data curation. **Wang Yue:** Resources, Writing - review & editing, Supervision, Data curation. **Zhang Hongfu:** Writing - review & editing. **Xu Shiwen:** Writing - review & editing.

Declaration of Competing Interest

The authors declare that they have no known competing financial interests or personal relationships that could have appeared to influence the work reported in this paper.

Acknowledgments

This research was supported by funds provided by China Agriculture Research System-41-17 and the National Key Research and Development Program of China (No. 2016YFD0500501).

Appendix A. Supplementary data

Supplementary material related to this article can be found, in the online version, at doi:https://doi.org/10.1016/j.jhazmat.2020.122605.

References

Adeva, M.M., Souto, G., Blanco, N., Donapetry, C., 2012. Ammonium metabolism in humans. Metabolism. 61, 1495–1511.
Chen, D., Miao, Z., Peng, M., Xing, H., Zhang, H., Teng, X., 2019a. The co-expression of

circRNA and mRNA in the thymuses of chickens exposed to ammonia. Ecotoxicol. Environ. Saf. 176, 146–152.
Chen, M., Li, X., Shi, Q., Zhang, Z., Xu, S., 2019b. Hydrogen sulfide exposure triggers chicken trachea inflammatory injury through oxidative stress-mediated FOS/IL8 signaling. J. Hazard. Mater. 368, 243–254.
Du, C., Zhang, B., He, Y., Hu, C., Ng, Q.X., Zhang, H., Ong, C.N., Lin, Zhifen, 2017. Biological effect of aqueous C60 aggregates on Scenedesmus obliquus revealed by transcriptomics and non-targeted metabolomics. J. Hazard. Mater. 324, 221–229.
Duan, J., Yu, Y., Li, Y., Jing, L., Yang, M., Wang, J., Li, Y., Zhou, X., Miller, M.R., Sun, Z., 2017. Comprehensive understanding of PM2.5 on gene and microRNA expression patterns in zebrafish (Danio rerio) model. Sci. Total Environ. 586, 666–674.
Gao, M., Chen, M., Li, C., Xu, M., Liu, Y., Cong, M., Sang, N., Liu, S., 2018. Long non-coding RNA MT1DP shunts the cellular defense to cytotoxicity through crosstalk with MT1H and RhoC in cadmium stress. Cell Discov. 4, 5.
Hoetelmans, R., van Slooten, H.J., Keijzer, R., Erkeland, S., van de Velde, C.J., Dierendonck, J.H., 2000. Bcl-2 and Bax proteins are present in interphase nuclei of mammalian cells. Cell Death Differ. 7, 384–392.
Jin, J., Wang, Y., Wu, Z., Hergazy, A., Lan, J., Zhao, L., Liu, X., Chen, N., Lin, L., 2017. Transcriptomic analysis of liver from grass carp (Ctenopharyngodon idellus) exposed to high environmental ammonia reveals the activation of antioxidant and apoptosis pathways. Fish Shellfish Immunol. 63, 444–451.
Karreth, F.A., Pandolfi, P.P., 2013. ceRNA cross-talk in cancer: when ce-bling rivalries go awry. Cancer Discov. 3, 1113–1121.
Kathyayani, S.A., Poornima, M., Sukumaran, S., Nagavel, A., Muralidhar, M., 2019. Effect of ammonia stress on immune variables of Pacific white shrimp Penaeus vannamei under varying levels of pH and susceptibility to white spot syndrome virus. Ecotoxicol. Environ. Saf. 184, 109626.
Ku, T., Ji, X., Zhang, Y., Li, G., Sang, N., 2016. PM2.5, SO2 and NO2 co-exposure impairs neurobehavior and induces mitochondrial injuries in the mouse brain. Chemosphere 163, 27–34.
Kusakabe, M., Kutomi, T., Watanabe, K., Emoto, N., Aki, N., Kage, H., Hamano, E., Kitagawa, H., Nagase, T., Sano, A., Yoshida, Y., Fukami, T., Murakawa, T., Nakajima, J., Takamoto, S., Ota, S., Fukayama, M., Yatomi, Y., Ohishi, N., Takai, D., 2010. Identification of G0S2 as a gene frequently methylated in squamous lung cancer by combination of in silico and experimental approaches. Int. J. Cancer 126, 1895–1902.
Le, T.D., Zhang, J., Liu, L., Li, J., 2017. Computational methods for identifying miRNA sponge interactions. Briefings Bioinf. 18, 577–590.
Li, M.J., Zhang, J., Liang, Q., Xuan, C., Wu, J., Jiang, P., Li, W., Zhu, Y., Wang, P., Fernandez, D., Shen, Y., Chen, Y., Kocher, J.A., Yu, Y., Sham, P.C., Wang, J., Liu, J.S., Liu, X.S., 2017. Exploring genetic associations with ceRNA regulation in the human genome. Nucleic Acids Res. 45, 5653–5665.
Li, X., Chen, M., Shi, Q., Zhang, H., Xu, S., 2019. Hydrogen sulfide exposure induces apoptosis and necroptosis through lncRNA3037/miR-15a/BCL2-A20 signaling in broiler trachea. Sci. Total Environ., 134296.
Li, W., Li, D., Kuang, H., Feng, X., Ai, W., Wang, Y., Shi, S., Chen, J., Fan, R., 2020. Berberine increases glucose uptake and intracellular ROS levels by promoting Sirtuin 3 ubiquitination. Biomed. Pharmacother. 121, 109563.
Liang, Z., Liu, R., Zhao, D., Wang, L., Sun, M., Wang, M., Song, L., 2016. Ammonia exposure induces oxidative stress, endoplasmic reticulum stress and apoptosis in hepatopancreas of pacific white shrimp (Litopenaeus vannamei). Fish Shellfish Immunol. 54, 523–528.
Liu, M., Huang, X., Song, Y., Tang, J., Cao, J., Zhang, X., Zhang, Q., Wang, S., Xu, T., Kang, L., Cai, X., Zhang, H., Yang, F., Wang, H., Yu, J.Z., Lau, A.K.H., He, L., Huang, X., Duan, L., Ding, A., Xue, L., Gao, J., Liu, B., Zhu, T., 2019. Ammonia emission control in China would mitigate haze pollution and nitrogen deposition, but worsen acid rain. Proc. Natl. Acad. Sci. U. S. A. 116, 7760–7765.
Matsunaga, N., Ikeda, E., Kakimoto, K., Watanabe, M., Shindo, N., Tsuruta, A., Ikeyama, H., Hamamura, K., Higashi, K., Yamashita, T., Kondo, H., Yoshida, Y., Matsuda, M., Ogino, T., Tokushige, K., Itcho, K., Furuichi, Y., Nakao, T., Yasuda, K., Doi, A., Amamoto, T., Aramaki, H., Tsuda, M., Inoue, K., Ojida, A., Koyanagi, S., Ohdo, S., 2016. Inhibition of G0/G1 switch 2 ameliorates renal inflammation in chronic kidney disease. EBioMedicine 13, 262–273.
Mutlu, E.A., Comba, I.Y., Cho, T., Engen, P.A., Yazici, C., Soberanes, S., Hamanaka, R.B., Nigdelioglu, R., Meliton, A.Y., Ghio, A.J., Budinger, G.R.S., Mutlu, G.M., 2018. Inhalational exposure to particulate matter air pollution alters the composition of the gut microbiome. Environ. Pollut. 240, 817–830.
Nichols, C.E., Shepherd, D.L., Knuckles, T.L., Thapa, D., Stricker, J.C., Stapleton, P.A., Minarchick, V.C., Erdely, A., Zeidler-Erdely, P.C., Alway, S.E., Nurkiewicz, T.R., Hollander, J.M., 2015. Cardiac and mitochondrial dysfunction following acute pulmonary exposure to mountaintop removal mining particulate matter. Am. J. Physiol. Heart Circ. Physiol. 309, H2017–2030.
Pavanello, S., Bonzini, M., Angelici, L., Motta, V., Pergoli, L., Hoxha, M., Cantone, L., Pesatori, A.C., Apostoli, P., Tripodi, A., Baccarelli, A., Bollati, V., 2016. Extracellular vesicle-driven information mediates the long-term effects of particulate matter exposure on coagulation and inflammation pathways. Toxicol. Lett. 259, 143–150.
Plautz, J., 2018. Piercing the haze. Science 361, 1060–1063.
Shi, Q., Wang, W., Chen, M., Zhang, H., Xu, S., 2019. Ammonia induces Treg/Th1 imbalance with triggered NF-kappaB pathway leading to chicken respiratory inflammation response. Sci. Total Environ. 659, 354–362.
Stokstad, E., 2014. Air pollution. Ammonia pollution from farming may exact hefty health costs. Science 343, 238.
Suzuki, H., Yanaka, A., Shibahara, T., Matsui, H., Nakahara, A., Tanaka, N., Muto, H., Momoi, T., Uchiyama, Y., 2002. Ammonia-induced apoptosis is accelerated at higher pH in gastric surface mucous cells. Am. J. Physiol. Gastrointest. Liver Physiol. 283, G986–995.
Tay, Y., Rinn, J., Pandolfi, P.P., 2014. The multilayered complexity of ceRNA crosstalk and competition. Nature 505, 344–352.
Tuzlak, S., Kaufmann, T., Villunger, A., 2016. Interrogating the relevance of mitochondrial apoptosis for vertebrate development and postnatal tissue homeostasis. Genes Dev. 30, 2133–2151.
Van Damme, M., Clarisse, L., Whitburn, S., Hadji-Lazaro, J., Hurtmans, D., Clerbaux, C., Coheur, P.F., 2018. Industrial and agricultural ammonia point sources exposed. Nature 564, 99–103.
Wang, Y., Tang, M., 2019. Integrative analysis of mRNAs, miRNAs and lncRNAs in urban particulate matter SRM 1648a-treated EA.hy926 human endothelial cells. Chemosphere 233, 711–723.
Wang, L., Wang, H., Hu, M., Cao, J., Chen, D., Liu, Z., 2009. Oxidative stress and apoptotic changes in primary cultures of rat proximal tubular cells exposed to lead. Arch. Toxicol. 83, 417–427.
Wang, J., Xing, J., Mathur, R., Pleim, J.E., Wang, S., Hogrefe, C., Gan, C.M., Wong, D.C., Hao, J., 2017. Historical trends in PM2.5-related premature mortality during 1990-2010 across the Northern hemisphere. Environ. Health Perspect. 125, 400–408.
Wang, S., Li, X., Wang, W., Zhang, H., Xu, S., 2019a. Application of transcriptome analysis: oxidative stress, inflammation and microtubule activity disorder caused by ammonia exposure may be the primary factors of intestinal microvilli deficiency in chicken. Sci. Total Environ. 696, 134035.
Wang, S., Chi, Q., Hu, X., Cong, Y., Li, S., 2019b. Hydrogen sulfide-induced oxidative stress leads to excessive mitochondrial fission to activate apoptosis in broiler myocardia. Ecotoxicol. Environ. Saf. 183, 109578.
Wang, W., Shi, Q., Wang, S., Zhang, H., Xu, S., 2019c. Ammonia regulates chicken tracheal cell necroptosis via the LncRNA-107053293/MiR-148a-3p/FAF1 axis. J. Hazard. Mater., 121626.
Wei, M.M., Zhou, Y.C., Wen, Z.S., Zhou, B., Huang, Y.C., Wang, G.Z., Zhao, X.C., Pan, H.L., Qu, L.W., Zhang, J., Zhang, C., Cheng, X., Zhou, G.B., 2016. Long non-coding RNA stabilizes the Y-box-binding protein 1 and regulates the epidermal growth factor receptor to promote lung carcinogenesis. Oncotarget 7, 59556–59571.
Welch, C., Santra, M.K., El-Assaad, W., Zhu, X., Huber, W.E., Keys, R.A., Teodoro, J.G., Green, M.R., 2009. Identification of a protein, G0S2, that lacks Bcl-2 homology domains and interacts with and antagonizes Bcl-2. Cancer Res. 69, 6782–6789.
Wu, Y., Gu, B., Erisman, J.W., Reis, S., Fang, Y., Lu, X., Zhang, X., 2016. PM2.5 pollution is substantially affected by ammonia emissions in China. Environ. Pollut. 218, 86–94.
Xu, J., Li, Y., Lu, J., Pan, T., Ding, N., Wang, Z., Shao, T., Zhang, J., Wang, L., Li, X., 2015. The mRNA related ceRNA-ceRNA landscape and significance across 20 major cancer types. Nucleic Acids Res. 43, 8169–8182.
Xu, J., Feng, L., Han, Z., Li, Y., Wu, A., Shao, T., Ding, N., Li, L., Deng, W., Di, X., Wang, J., Zhang, L., Li, X., Zhang, K., Cheng, S., 2016. Extensive ceRNA-ceRNA interaction networks mediated by miRNAs regulate development in multiple rhesus tissues. Nucleic Acids Res. 44, 9438–9451.
Yang, T., Cao, C., Yang, J., Liu, T., Lei, X.G., Zhang, Z., Xu, S., 2018. miR-200a-5p regulates myocardial necroptosis induced by Se deficiency via targeting RNF11. Redox Biol. 15, 159–169.
Yang, J., Gong, Y., Cai, J., Liu, Q., Zhang, Z., 2019. Lnc-3215 suppression leads to calcium overload in selenium deficiency-induced chicken heart lesion via the lnc-3215-miR-1594-TNN2 pathway. Mol. Ther. Nucleic Acids 18, 1–15.
Yim, C.Y., Sekula, D.J., Hever-Jardine, M.P., Liu, X., Warzecha, J.M., Tam, J., Freemantle, S.J., Dmitrovsky, E., Spinella, M.J., 2016. G0S2 suppresses oncogenic transformation by repressing a MYC-regulated transcriptional program. Cancer Res. 76, 1204–1213.
Yim, C.Y., Bikorimana, E., Khan, E., Warzecha, J.M., Shin, L., Rodriguez, J., Dmitrovsky, E., Freemantle, S.J., Spinella, M.J., 2017. G0S2 represses PI3K/mTOR signaling and increases sensitivity to PI3K/mTOR pathway inhibitors in breast cancer. Cell Cycle 16, 2146–2155.
Zeng, N., Wang, T., Chen, M., Yuan, Z., Qin, J., Wu, Y., Gao, L., Shen, Y., Chen, L., Wen, F., 2019. Cigarette smoke extract alters genome-wide profiles of circular RNAs and mRNAs in primary human small airway epithelial cells. J. Cell. Mol. Med. 23, 5532–5541.
Zhang, J., Li, C., Tang, X., Lu, Q., Sa, R., Zhang, H., 2015. High concentrations of atmospheric ammonia induce alterations in the hepatic proteome of broilers (Gallus Gallus): an iTRAQ-based quantitative proteomic analysis. PLoS One 10, e0123596.
Zhang, L., Cheng, H., Yue, Y., Li, S., Zhang, D., He, R., 2018. H19 knockdown suppresses proliferation and induces apoptosis by regulating miR-148b/WNT/beta-catenin in ox-LDL -stimulated vascular smooth muscle cells. J. Biomed. Sci. 25, 11.
Zhou, Z., Zhu, Y., Gao, G., Zhang, Y., 2019. Long noncoding RNA SNHG16 targets miR-146a-5p/CCL5 to regulate LPS-induced WI-38 cell apoptosis and inflammation in acute pneumonia. Life Sci. 228, 189–197.